RSC Advances

PAPER

View Article Online
View Journal | View Issue

Check for updates

Cite this: *RSC Adv.*, 2021, **11**, 10309

$SrTi(IO_3)_6 \cdot 2H_2O$ and $SrSn(IO_3)_6$: distinct arrangements of lone pair electrons leading to large birefringences†

Kaitong Liu,[ab] Jian Han,[*a] Junben Huang,[a] Zhonglei Wei,[ab] Zhihua Yang[a] and Shilie Pan[*a]

Received 22nd December 2020
Accepted 3rd March 2021

DOI: 10.1039/d0ra10726c

rsc.li/rsc-advances

Three new iodates $SrTi(IO_3)_6 \cdot 2H_2O$, $(H_3O)_2Ti(IO_3)_6$, and $SrSn(IO_3)_6$ have been synthesized *via* a facile hydrothermal method. The three compounds have zero-dimensional crystal structures composed of one $[MO_6]^{8-}$ (M = Ti, Sn) octahedron connected with six $[IO_3]^-$ trigonal pyramids. However, the particular coordination of Sr^{2+} cations results in distinct arrangements of lone pair electrons in an $[IO_3]^-$ trigonal pyramid, which leads to large birefringences. More importantly, this work enriches the species crystal chemistry for $[M(IO_3)_6]^{2-}$ (M = Ti, Sn) clusters-containing iodates.

Introduction

For a compound, the structure determines its physicochemical properties and the fields of potential applications.[1,2] And a lot of high-performance iodate compounds have been reported owing to the unique arrangements of I–O anion groups, such as NaI_3O_8, $Bi(IO_3)F_2$, $Cs_2I_4O_{11}$, $ABi_2(IO_3)_2F_5$ (A = K, Rb, Cs), $LiM^{II}(IO_3)_3$ (M^{II} = Zn and Cd), and AgI_3O_8.[3] There are two types of coordination modes for I^{5+} cations ($[IO_3]^-$ and $[IO_4]^{3-}$) since the weak I–O interactions will be neglected if the I–O bond lengths are larger than 2.4 Å, which result in the limited structural diversity of metal iodates.[3f]

Therefore, some metal cations (Ti^{4+}, V^{5+}, Cr^{6+}, Pt^{4+}, Ge^{4+}, Sn^{4+}, Mo^{6+}, Mo^{4+}, Zr^{4+}, and Nb^{5+}) and nonmetal cations (Se^{4+} and Te^{4+}) have been introduced into iodates to enrich the structural chemistry and enhance the properties.[4] And interestingly, through introducing homo-valence Mo^{4+}, Zr^{4+}, Ge^{4+}, Ti^{4+}, Pt^{4+}, and Sn^{4+} metal cations into iodates, the similar $[M(IO_3)_6]^{2-}$ clusters (M = Mo, Zr, Ge, Ti, Pt, and Sn) can be formed, which possess $[MO_6]^{8-}$ (M = Mo, Zr, Ge, Ti, Pt, and Sn) octahedron connected with six $[IO_3]^-$ trigonal pyramids. The $[M(IO_3)_6]^{2-}$ clusters (M = Mo, Zr, Ge, Ti, Pt, and Sn) can be isostructural when they have the same arrangement of $[IO_3]^-$ trigonal pyramids, which will be isostructural for metal iodates.[4a,e,h,5]

Moreover, the birefringence of iodates has also been comprehensively studied due to the stereochemical activity of the lone pair (SCALP) of I^{5+} in the $[IO_3]^-$ group. The SCALP should be considered as a vital factor to influence the birefringence, such as Sn^{2+} with SCALP enhancing the birefringence in $BaSn_2(PO_4)_2$ and $Sn_2B_5O_9Cl$.[6] While for iodates, the I^{5+} cation with SCALP in the $[IO_3]^-$ group can also influence the birefringence apparently when the $[IO_3]^-$ groups are arranged regularly. And introducing $[IO_3]^-$ groups into borates and phosphates can significantly increase the birefringence such as metal borate-iodates $Sr[B(OH)_4](IO_3)$ and $Li_4Sr_5[B_{12}O_{22}(OH)_4](IO_3)_2$, as well as the metal iodate-phosphate $Pb_2(IO_3)(PO_4)$.[7]

Herein, three new Ti^{4+} or Sn^{4+}-containing iodates, $SrTi(IO_3)_6 \cdot 2H_2O$ (**1**), $(H_3O)_2Ti(IO_3)_6$ (**2**), and $SrSn(IO_3)_6$ (**3**) were synthesized through the mild hydrothermal method. And all of them possess zero-dimensional crystal structures which are composed of $[M(IO_3)_6]^{2-}$ (M = Ti, Sn) clusters and cations filling in voids among the $[M(IO_3)_6]^{2-}$ (M = Ti, Sn) clusters. The $[M(IO_3)_6]^{2-}$ (M = Ti, Sn) cluster consists of $[MO_6]^{8-}$ (M = Ti, Sn) octahedra connected with six $[IO_3]^-$ trigonal pyramids through sharing vertex O atoms. They are not isostructural although crystalizing in centrosymmetric space group $R\bar{3}$ (No. 148). Whereas, the particular coordination of Sr^{2+} cations filling in voids leads to the distinct arrangements of lone pair electrons in the $[IO_3]^-$ trigonal pyramids and results in large birefringences. More importantly, compounds **1** and **2** are enriching the species of $[Ti(IO_3)_6]^{8-}$ groups and crystal water molecules-containing iodates. Compound **3** is the first alkaline-earth metal and $[Sn(IO_3)_6]^{8-}$ groups-containing iodate.

[a]*CAS Key Laboratory of Functional Materials and Devices for Special Environments, Xinjiang Technical Institute of Physics & Chemistry, CAS, Xinjiang Key Laboratory of Electronic Information Materials and Devices, 40-1 South Beijing Road, Urumqi 830011, China. E-mail: hanjian@ms.xjb.ac.cn; slpan@ms.xjb.ac.cn*

[b]*Center of Materials Science and Optoelectronics Engineering, University of Chinese Academy of Sciences, Beijing 100049, China*

† Electronic supplementary information (ESI) available: The final refined atomic positions, isotropic thermal parameters table and BVS; the selected bond distances and bond angles; experimental and calculated powder X-ray diffraction patterns, comparison of structures, TG-DSC curves, IR spectra, calculated birefringence and the contribution of the functional groups to birefringence; the arrangements diagrammatic drawing of lone pair electrons. CCDC 2014017, 2014302 and 2042263 for $SrTi(IO_3)_6 \cdot 2H_2O$, $(H_3O)_2Ti(IO_3)_6$ and $SrSn(IO_3)_6$, respectively. For ESI and crystallographic data in CIF or other electronic format see DOI: 10.1039/d0ra10726c

Open Access Article. Published on 10 March 2021. Downloaded on 7/31/2024 3:28:18 PM.
This article is licensed under a Creative Commons Attribution-NonCommercial 3.0 Unported Licence.

Open Access Article. Published on 10 March 2021. Downloaded on 7/31/2024 3:28:18 PM.
This article is licensed under a Creative Commons Attribution-NonCommercial 3.0 Unported Licence.

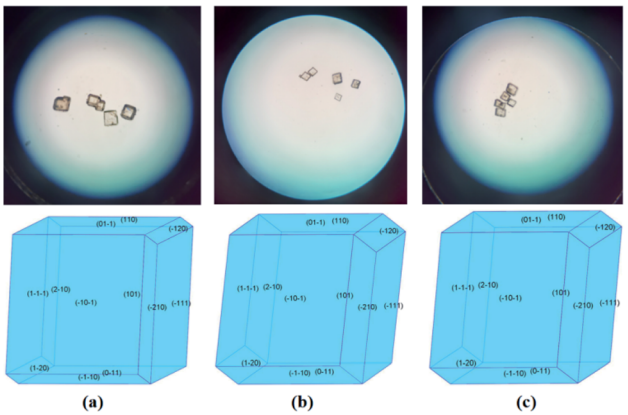

Fig. 1 The grown crystal grains and simulated morphologies of (a) $SrTi(IO_3)_6 \cdot 2H_2O$, (b) $(H_3O)_2Ti(IO_3)_6$, and (c) $SrSn(IO_3)_6$, respectively.

Experimental section

Crystal growth

$Sr(OH)_2 \cdot 8H_2O$ (0.034 g) (Aladdin Industrial Co., Ltd., 99.5%), HIO_3 (0.446 g) (Aladdin Industrial Co., Ltd., 99.5%), TiO_2 (Tianjin Fuchen Chemical Co., Ltd., 99%), and SnO (Aladdin Industrial Co., Ltd., 99.5%) were used as received from commercial sources without any further purification.

The starting reagents are $Sr(OH)_2 \cdot 8H_2O$ (0.034 g), TiO_2 (0.020 g), HIO_3 (0.446 g) for compound **1**, TiO_2 (0.022 g), HIO_3 (0.478 g) for compound **2** and $Sr(OH)_2 \cdot 8H_2O$ (0.056 g), SnO (0.059 g), HIO_3 (0.383 g) for compound **3**, which are mixed respectively and put into PTFE pouches. Then these pouches were enclosed in 120 mL autoclaves with PTFE inner linings and added 15 mL of deionized water and heated at 190 °C for 3 days. The pouches were cooled at a rate of 0.6 °C h^{-1} to 130 °C and then 1 °C h^{-1} to room temperature. After cleaned with deionized water, the colorless block crystals were obtained. Crystal samples can also be obtained based on the following reaction:

$$Sr(OH)_2 \cdot 8H_2O + TiO_2 + 6HIO_3 \rightarrow SrTi(IO_3)_6 + 12H_2O$$

$$TiO_2 + 6HIO_3 \rightarrow (H_3O)_2Ti(IO_3)_6$$

$$2Sr(OH)_2 \cdot 8H_2O + 2SnO + 12HIO_3 + O_2 \rightarrow 2SrSn(IO_3)_6 + 24H_2O$$

Fig. 1 shows the photos of grown crystal grains and the simulated morphologies of the compounds. On the basis of the crystal structure, the theoretical morphology can be calculated through the Bravais–Friedel–Donnay–Harker (BFDH) theory.[8] The grown crystals are in line with the simulated morphologies.

Single-crystal X-ray crystallography

The single crystals selected manually are mounted on thin glass fibers using epoxy for data collection. The diffraction data collection of these compounds was conducted on a Bruker SMART APEX II CCD diffractometer with a Mo Kα radiation (λ = 0.71073 Å) at room temperature. And the data were integrated *via* SAINT, and then the crystal structures were solved with the direct method and refined by full-matrix least-squares fitting on F^2 using the SHELX.[9] The PLATON software verifies no other missed symmetry existed.[10] The crystal information and structure refinements are recorded in Table 1. The atomic coordinates, equivalent isotropic displacement parameters, bond valence sum (BVS), and selected bond lengths and angles are given in Tables S1 and S2.†

Powder X-ray diffraction

X-ray diffraction (XRD) measurements were carried out on a Bruker D2 PHASER diffractometer equipped with a diffracted beamed monochromator set for Cu Kα (λ = 1.54056 Å) radiation at room temperature in the 2θ range from 10 to 70° with a scan step width of 0.02° and a fixed counting time of 1 s per step. The experimental powder XRD patterns are well in agreement with the simulated ones (Fig. 2).

Infrared and Raman spectrum

The samples and dried KBr were mixed completely in the molar ratio of 1 : 100 and then pressed into a thin wafer to collect the infrared

Table 1 Crystal data and structure refinement for $SrTi(IO_3)_6 \cdot 2H_2O$, $(H_3O)_2Ti(IO_3)_6$, and $SrSn(IO_3)_6$, respectively

Empirical formula	$SrTi(IO_3)_6 \cdot 2H_2O$	$(H_3O)_2Ti(IO_3)_6$	$SrSn(IO_3)_6$
Formula weight	1220.95	1135.35	1255.71
Crystal system		Trigonal	
Space group		$R\bar{3}$	
a/Å	11.3720(11)	11.31(3)	10.807(7)
b/Å	12.5321(19)	11.36(3)	11.098(7)
Volume/Å^3	1403.6(3)	1258(7)	1122.5(16)
Z, ρ calcd/g cm^{-3}	3, 4.334	3, 4.495	3, 5.573
Theta range for data collection/°	2.630 to 27.318	2.746 to 27.189	2.847 to 27.422
Reflections collected/unique	2867/704 [R(int) = 0.0390]	2567/628 [R(int) = 0.0501]	2340/576 [R(int) = 0.0354]
Completeness	99.90%	100.00%	100.00%
Goodness-of-fit on F^2	1.053	0.977	1.095
Final R indices [I > 2sigma(I)][a]	R_1 = 0.0191, wR_2 = 0.0380	R_1 = 0.0259, wR_2 = 0.0360	R_1 = 0.0172, wR_2 = 0.0366
R Indices (all data)[a]	R_1 = 0.0221, wR_2 = 0.0390	R_1 = 0.0361, wR_2 = 0.0382	R_1 = 0.0196, wR_2 = 0.0374
Extinction coefficient	0.00224(7)	0.00038(4)	0.00128(7)
Largest diff. Peak and hole/e Å^{-3}	0.808 and −0.596	0.740 and −0.877	0.870 and −0.707

[a] $R_1 = \Sigma||F_o| - |F_c||/\Sigma|F_o|$ and $wR_2 = [\Sigma w(F_o^2 - F_c^2)^2/\Sigma wF_o^4]^{1/2}$ for $F_o^2 > 2\sigma(F_o^2)$.

© 2021 The Author(s). Published by the Royal Society of Chemistry

Open Access Article. Published on 10 March 2021. Downloaded on 7/31/2024 3:28:18 PM.
This article is licensed under a Creative Commons Attribution-NonCommercial 3.0 Unported Licence.

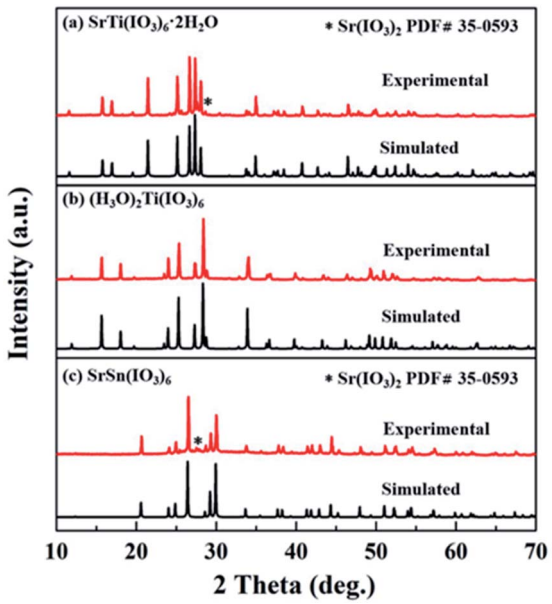

Fig. 2 Experimental and calculated powder X-ray diffraction patterns of (a) $SrTi(IO_3)_6{\cdot}2H_2O$, (b) $(H_3O)_2Ti(IO_3)_6$, and (c) $SrSn(IO_3)_6$, respectively.

(IR) spectra through a Shimadzu IRAffinity-1 spectrometer. The samples were ground thoroughly and pressed to flat for collecting the Raman spectra on a LabRAM HR evolution equipment.

UV-vis-NIR transmission and photoluminescence spectrum

The UV-vis-NIR diffuse reflectance spectra were characterized *via* a Shimadzu SolidSpec-3700DUV spectrophotometer. The function $F(R) = (1 - R)^2/2R$ is applied to convert the reflectance spectra, where R is the reflectance and $F(R)$ is the Kubelka–Munk remission function.[11] Photoluminescence (PL) spectra were performed *via* FLS1000-Edinburgh Instruments.

Thermal and magnetically analysis

Using a NETZSCH STA 449C simultaneous thermal analyzer, compounds **1**, **2**, and **3** were placed in the platinum crucibles and heated from 40 to 1000, 500, and 800 °C at a rate of 5 °C min^{-1} under a flow of N_2 to get TG and DSC data, respectively. Magnetic properties of the samples were performed by the DC magnetization measurements using a vibrating sample magnetometer (VSM, QUANTUM DESIGN).

Birefringent measurement

A polarizing microscope (ZEISS Axio Scope. A1) was used to study the birefringences (Δn) with a visible light filter at 546 nm. The optical path difference (R) was quantified under the cross-polarized light based on the maximum interference color.[12] The formula for calculating the birefringence is

$$R = |N_e - N_o| \times d = \Delta n \times d,$$

where N_e and N_o represent the refractive indexes of light through a crystal.

Theoretical calculations

To deeply explore the origin of optical properties, the first-principles calculation was carried out to simulate electron and band structures along with birefringence by the plane-wave pseudopotential method embedding in the CASTEP package.[13] The Perdew–Burke–Ernzerhof functional within the generalized gradient approximation was applied for the exchange–correlation potential.[14] The plane-wave cutoff energy was set at 830 eV with a separation of Monkhorst–Pack k-point sampling of 0.04 $Å^{-1}$ for the aim of energy convergence.

Results and discussion

Crystal structure

Compound **1** crystallizes in a centrosymmetric trigonal space group $R\bar{3}$ (No. 148) with $a = 11.3720(11)$ Å, $c = 12.5321(19)$ Å, and $Z = 3$, however, it is not isostructural to $BaTi(IO_3)_6$, and $A_2Ti(IO_3)_6$ (A = K, Rb, Cs, and Tl).[5b,d] There is one unique Sr atom, one unique Ti atom, one unique I atom, four unique O atoms, and two H atoms in the asymmetric unit. The Ti^{4+} cation is coordinated to six O atoms, forming the $[TiO_6]^{8-}$ octahedron which is linked to six $[IO_3]^-$ trigonal pyramids, and further forms a $[Ti(IO_3)_6]^{2-}$ group (Fig. 3a). The Ti–O bonds have a unique distance of 1.915(3) Å. The I^{5+} cations are coordinated to three O atoms in a distorted trigonal pyramidal with I–O bond lengths ranging from 1.790(3) to 1.843(3) Å. The Sr^{2+} cations are coordinated with eight O atoms to form a hexagonal bipyramid with six equatorial oxygen atoms (Fig. S2a†). The pyramid with Sr–O distances of 2.433(8)–2.664(3) Å, resides in the site formed by eight $[Ti(IO_3)_6]^{2-}$ groups. Bond valence sum (BVS) values were calculated to check the reliability of each atom (Table S1†).[15] Only the bond valence of O1 (0.42) is not regular, so two hydrogen atoms should be coordinated to O1 to balance the bond valence. It should be noted that the one H^+ cation is disordered over three sites with 66.7% occupancy on each site resulting from the three-fold axis through the O1 atom (Fig. 3b). The two $[Ti(IO_3)_6]^{2-}$ units are separated by one Sr^{2+} cation and two H_2O molecules (Fig. 3c), and further form the zero-dimensional structure of compound **1** (Fig. 3d).

Compounds **2** and **3** also crystallize in centrosymmetric trigonal space groups $R\bar{3}$ (No. 148) and have similar structures

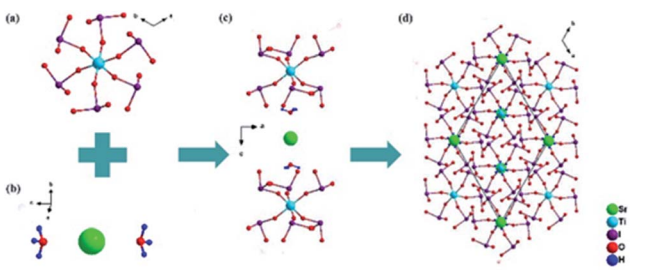

Fig. 3 Ball and stick structure of $SrTi(IO_3)_6{\cdot}2H_2O$. (a) The basic building unit $[Ti(IO_3)_6]^{2-}$ of $SrTi(IO_3)_6{\cdot}2H_2O$. (b) The Sr^{2+} cation and H_2O molecules. (c) Two $[Ti(IO_3)_6]^{2-}$ units separated by one Sr^{2+} cation and two H_2O molecules. (d) The final zero-dimensional structure of $SrTi(IO_3)_6{\cdot}2H_2O$.

© 2021 The Author(s). Published by the Royal Society of Chemistry

Open Access Article. Published on 10 March 2021. Downloaded on 7/31/2024 3:28:18 PM.
This article is licensed under a Creative Commons Attribution-NonCommercial 3.0 Unported Licence.

to compound **1** (Fig. S1 and S2†), so the detailed structures are not demonstrated here. And compound **2** is isostructural to β-$(H_3O)_2Pt(IO_3)_6$ reported by Mao's group.[5c] And compound **3** is not isostructural to $A_2Sn(IO_3)_6$ (A = K, Rb, Cs) and $Sn^{2+}Sn^{4+}(IO_3)_6$.

Compounds **1**, **2**, and **3** possess the different arrangements of $[M(IO_3)_6]^{2-}$ (M = Ti, Sn) groups even though all crystallize in the same space group $R\bar{3}$. Owing to the unique M–O (M = Ti, Sn) bond distances in each compound, the $[MO_6]^{8-}$ (M = Ti, Sn) octahedra have no out of center distortion.[16] So the main difference is the condition of $[IO_3]^-$ trigonal pyramid. Each I^{5+} cation in these compounds is bonded to three oxygen atoms, and owing to its lone electron pair, an $[IO_3]^-$ trigonal pyramidal coordination environment is observed. For compound **1**, the planes formulated *via* three oxygen atoms in $[IO_3]^-$ trigonal pyramid have two angle values (41.264 and 48.736°) with the *c*-axis in each compound (Fig. 4a). However, for compounds **2** and **3**, the corresponding unique angle values are 8.296 and 30.384° with the *c*-axis, respectively (Fig. 4b and c). From Fig. S3,† except hydrogen atoms, there are two oxygen atoms and one strontium atom between the two adjacent $[M(IO_3)_6]^{2-}$ (M = Ti, Sn) groups for compound **1**, while there are two oxygen atoms for compound **2** as well as one strontium atom for compound **3**. The particular hexagonal bipyramid coordination of Sr^{2+} in compound **1** (Fig. S4a†) should result in taking up the place between the two H_2O molecules (Fig. S3a†). And in order to maintain this coordination for compound **1**, the arrangements of $[IO_3]^-$ should rotate with respect to the $[TiO_6]^{8-}$ octahedron, in which the rotation aligns the polarization from the $[IO_3]^-$ groups in opposite directions. Alike to compound **1**, in order to sustain special Sr^{2+} bipyramid coordination in compound **3** (Fig. S4b†), the arrangements of $[IO_3]^-$ should rotate taking account of the $[SnO_6]^{8-}$ octahedron (Fig. S3b†). So the angles of compounds **1** and **3** mentioned above are larger than that of compound **2**.

IR and Raman spectroscopy

The IR and Raman spectra are shown in Fig. S5.† For compounds **1**, and **2**, IR spectra are similar except for the absorption bands at 2358 cm^{-1} in compound **2**, which are caused by bending modes of H–O–H units.[17] The IR absorption bands at 3500–2800 cm^{-1} can be assigned to the stretching vibrations of the H_2O band, the absorption bands at 1850–1000 cm^{-1} are consistent with the bending and stretching vibrations of the H–O–H units.[17] The absorption bands in the range of 890–750 cm^{-1} and 490–400 cm^{-1} are consistent with stretching and bending vibrations of the I–O groups.[18] The IR absorption bands at 700, 704, and 671 cm^{-1} in the three compounds are caused by the $[MO_6]^{8-}$ (M = Ti, Sn) units stretching vibrations.[5b] The Raman spectra were used to further verify the existence of the $[M(IO_3)_6]^{2-}$ (M = Ti, Sn) groups. The proposed assignments of observed positions of the Raman bands are illustrated in Table S4,† which are consistent with the reported results.[19]

UV-vis-NIR transmission and photoluminescence spectrum

Fig. 5a–c displays the UV-vis-NIR diffuse reflectance spectra. The cut-off edges of compounds **1**, **2**, and **3** are 318, 330, and 250 nm (inset of Fig. 5a–c), and the corresponding energy gaps are 3.38, 3.35, and 4.08 eV, respectively, which are close to those of the previously reported iodate crystals.[5f,20] Fig. 5d shows the photoluminescence emission spectrum of the three compounds. The bands around 300 nm (4.13 eV) can be in corresponding with a result of ground state to their excited state electronic transitions. Photoluminescence in two broad bands at 360 nm (3.44 eV) for compound **3** and 370 nm (3.35 eV) for compounds **1** and **2** are associated with electronic transitions from the ground state to the conduction band selftrapped excitons, and the bands around 470 nm (2.64 eV) and 560 nm (2.21 eV) are excited most effectively at short wavelengths.[21]

Thermal and magnetic properties

The TG-DSC curves of the three compounds are shown in Fig. S6.† There are four remarkably endothermic peaks at 350, 450, 477, and 595 °C for compound **1**, respectively (Fig. S6a†). In the range of 220–370 °C, there is a mass loss of 2.9%, which is consistent with the loss of two molecules of H_2O with a calculated value of 3.0%.[22] The TG curve in the range of 370–1000 °C shows a total mass loss of 80.9%, which corresponds to the decomposition process of three I_2O_5 molecules.[23] The loss is consistent with the calculated value of 82.0%.

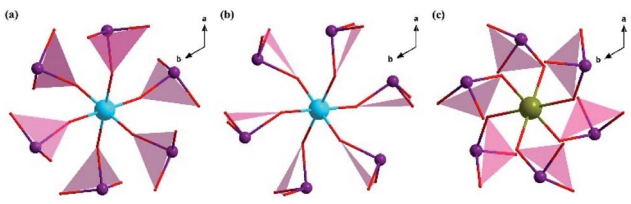

Fig. 4 From the *c*-axis direction, the condition of planes formed by three O atoms in $[IO_3]^-$ trigonal pyramid of a $[Ti(IO_3)_6]^{2-}$ group for (a) $SrTi(IO_3)_6{\cdot}2H_2O$, (b) $(H_3O)_2Ti(IO_3)_6$ and (c) $SrSn(IO_3)_6$, respectively.

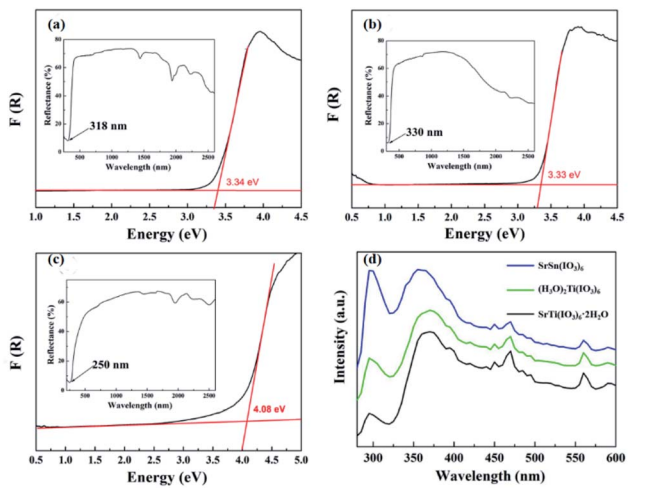

Fig. 5 Optical absorption spectra of (a) $SrTi(IO_3)_6{\cdot}2H_2O$, (b) $(H_3O)_2Ti(IO_3)_6$, and (c) $SrSn(IO_3)_6$ as well as (d) PL spectra of the compounds.

© 2021 The Author(s). Published by the Royal Society of Chemistry

Open Access Article. Published on 10 March 2021. Downloaded on 7/31/2024 3:28:18 PM.
This article is licensed under a Creative Commons Attribution-NonCommercial 3.0 Unported Licence.

There are three distinct endothermic peaks at 220, 409, and 458 °C for compound **2** (Fig. S6b†). In the range of 120–227 °C it has a mass loss of 4.8%, which is consistent with the loss of three molecules of H_2O with a calculated value of 4.7%.[22] And there is a mass loss of 90.7% in the range of 227–500 °C, which is consistent with the decomposition process of three I_2O_5 molecules.[23] The loss is consistent with the calculated value of 88.3%.

There are two distinct endothermic peaks at 492 and 566 °C for compound **2** (Fig. S6c†). And there is a mass loss of 80.8% in the range of 440–800 °C, which is consistent with the decomposition process of three I_2O_5 molecules.[23] The loss is consistent with the calculated value of 79.8%.

The field-dependent magnetization plots are displayed in Fig. S7,† which shows that the three compounds are a para/antimagnetic nature at a low and high field.[19g] It has been reported that the $SrTiO_3$ and $SrSnO_3$ are diamagnetic.[19g,24] Whereas, the para/antimagnetism of these compounds may come from introducing $[IO_3]^-$ anion groups and further compensating the diamagnetism of inner electrons.

Theoretical calculations and birefringent analysis

The electronic structures of the three compounds are shown in Fig. 6. Compounds **1**, **2**, and **3** possess indirect band gaps of 2.50, 2.62, and 3.19 eV, respectively, which are always smaller than the experimental values.[25] And from the PDOS of compounds **1** and **2**, the bottom of conduction bands is mainly contributed by Ti-3d, I-5p, and O-2p states and the top of the valence bands mainly comes from I-5p, O-2p states. Moreover, for compound **3**, the I-5p, O-2s, and O-2p states mainly determine both the bottom of conduction bands and the top of the valence bands. In other words, the $[Ti(IO_3)_6]^{2-}$ groups determine the Fermi level position of compounds **1** and **2**, while the $[IO_3]^-$ groups for compound **3**.

The calculated birefringence values of compounds **1**, **2**, and **3** are shown in Fig. S8a.† Thereinto, compounds **1** and **3** possess larger birefringences compared to compound **2**. Furthermore, the Δn values of compounds **1**, **2**, and **3** were measured by a ZEISS Axio Scope polarizing microscope (Table 2). According to the results, the retardations are about 1331, 906, and 2690 nm for compounds **1**, **2**, and **3**, respectively. So the approximate experimental values of 0.093, 0.045, and 0.116 at 546 nm for these three compounds are consistent with the calculated results and verify the rationality of the calculations.

It is well known that the optical properties depend on the hybridization of electron orbitals around Femi level, which states that the birefringence is mainly affected by the response electron distribution of the $[Ti(IO_3)_6]^{2-}$ and $[IO_3]^-$ groups for compounds **1**, **2** and **3**, respectively. Moreover, the $[TiO_6]^{8-}$ octahedra in each compound are not out of center distortion, and therefore, the difference of $[IO_3]^-$ in $[Ti(IO_3)_6]^{2-}$ groups plays a dominant role on the different birefringence, as the influence of $[TiO_6]^{8-}$ octahedra can be in a little scale. To further analyze the $[IO_3]^-$ groups to be the dominant factor on the amplification of birefringence, a real-space atom-cutting method was adopted for compounds **1** and **2** (Fig. S8(b) and (c)†). And for compound **3**, we have tried many times and failed to get a reasonable result. From the PDOS of compound **3**, the hybridization of $[IO_3]^-$ trigonal pyramid is the main contribution to optical properties as well as birefringence. The condition of lone pair electrons in $[IO_3]^-$ trigonal pyramid can be associated with the orientation of the plane formulated by three oxygen atoms. Meanwhile, it is known that the *c*-axis of the three compounds is the optical principle axis because they all crystalize in $R\bar{3}$ space group. For compounds **1** and **3**, half of the lone pair electrons can be regarded as inclining to the positive *c*-axis in a large degree, and the rest to negative (Fig. S9a and c†). While, from the *c*-axis direction, the lone pair electrons of compound **2** are inclined to the positive or negative *c*-axis in a tiny magnitude (Fig. S9b†). These different arrangements of lone pair electrons may induce large birefringences for compounds **1** and **3** compared to compound **2**. Besides, the

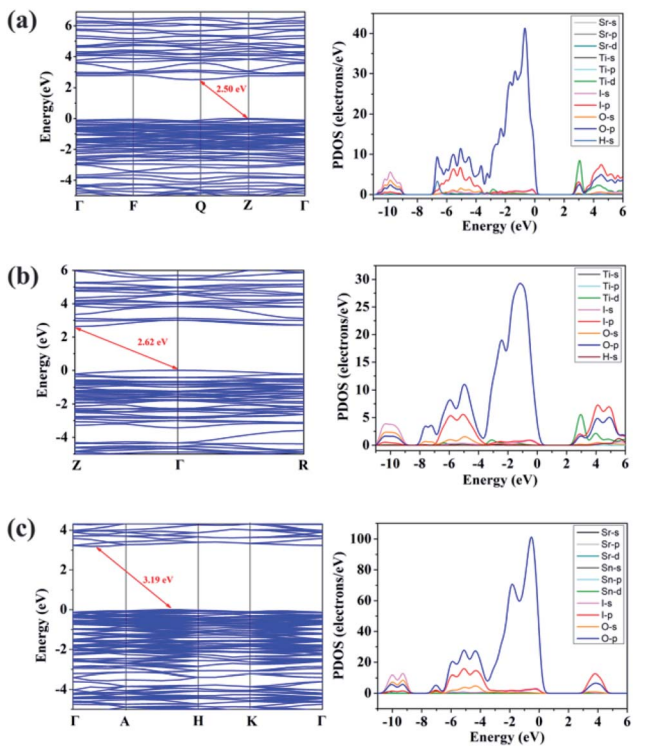

Fig. 6 Band gaps, the partial density of states (PDOS) of (a) $SrTi(IO_3)_6\cdot 2H_2O$, (b) $(H_3O)_2Ti(IO_3)_6$, and (c) $SrSn(IO_3)_6$.

Table 2 Calculated and experimental birefringences at 546 nm of the three compounds and the contributions for birefringence of each functional group of $SrTi(IO_3)_6\cdot 2H_2O$, and $(H_3O)_2Ti(IO_3)_6$ at the static limit derived from the cut-TiO group wave functions and cut-IO group wave functions

Birefringence	$SrTi(IO_3)_6\cdot 2H_2O$	$(H_3O)_2Ti(IO_3)_6$	$SrSn(IO_3)_6$
Experimental	0.093	0.045	0.116
Calculated	0.109	0.038	0.128
IO group	0.081	0.04	—
TiO group	0.018	0.035	—

Open Access Article. Published on 10 March 2021. Downloaded on 7/31/2024 3:28:18 PM.
This article is licensed under a Creative Commons Attribution-NonCommercial 3.0 Unported Licence.

higher density of $[IO_3]^-$ in compound **3** may lead to a larger birefringence than compound **1** (the unit cell volume of compound **1** (1403.6(3) Å^3) is larger than that of compound **3** (1122.5(16) Å^3)).

Conclusion

In summary, three iodates, $SrTi(IO_3)_6 \cdot 2H_2O$, $(H_3O)_2Ti(IO_3)_6$, and $SrSn(IO_3)_6$, have been obtained successfully *via* the facile hydrothermal method. They crystallize in centrosymmetric space groups $R\bar{3}$ and possess zero-dimensional structures with isolated $[M(IO_3)_6]^{2-}$ (M = Ti, Sn) that are composed of $[MO_6]$ octahedra connected to six $[IO_3]^-$ trigonal pyramids. The introduction of the Sr^{2+} cation results in the different arrangements of $[IO_3]^-$ trigonal pyramids. The distinct arrangements of lone pair electrons of the I^{5+} cation lead to larger birefringences in $SrTi(IO_3)_6 \cdot 2H_2O$ and $SrSn(IO_3)_6$ than that in $(H_3O)_2Ti(IO_3)_6$. And this work enriches the species crystal chemistry for $[M(IO_3)_6]^{2-}$ (M = Ti, Sn) clusters-containing iodates.

Conflicts of interest

There are no conflicts of interest to declare.

Acknowledgements

This work was financially supported by the West Light Foundation of the Chinese Academy of Sciences (2020-XBQNXZ-002), National Natural Science Foundation of China (U2003131, 51972336, 61835014, 11774414), Natural Science Foundation of Xinjiang, China (2019D01A93), Tianshan Youth Program of Xinjiang (2018Q035), and Tianshan Innovation Team Program (2018D14001).

References

1 (*a*) B. C. Wu, D. Y. Tang, N. Ye and C. T. Chen, *Opt. Mater.*, 1996, **5**, 105–109; (*b*) W. J. Yao, R. He, X. Y. Wang, Z. S. Lin and C. T. Chen, *Adv. Opt. Mater.*, 2014, **2**, 411–417; (*c*) Y. Wang and S. L. Pan, *Coord. Chem. Rev.*, 2016, **323**, 15–35; (*d*) G. Q. Shi, Y. Wang, F. F. Zhang, B. B. Zhang, Z. H. Yang, X. L. Hou, S. L. Pan and K. R. Poeppelmeier, *J. Am. Chem. Soc.*, 2017, **139**, 10645–10648; (*e*) B. B. Zhang, G. Q. Shi, Z. H. Yang, F. F. Zhang and S. L. Pan, *Angew. Chem., Int. Ed.*, 2017, **56**, 3916–3919; (*f*) G. Y. Yang and K. C. Wu, *Inorg. Chem.*, 2018, **57**, 7503–7506; (*g*) M. Mutailipu and S. L. Pan, *Angew. Chem., Int. Ed.*, 2020, **59**, 20302–20317; (*h*) H. P. Wu, S. L. Pan, K. R. Poeppelmeier, H. Y. Li, D. Z. Jia, Z. H. Chen, X. Y. Fan, Y. Yang, J. M. Rondinelli and H. S. Luo, *J. Am. Chem. Soc.*, 2011, **133**, 7786–7790.

2 (*a*) Y. Wang, B. B. Zhang, Z. H. Yang and S. L. Pan, *Angew. Chem., Int. Ed.*, 2018, **57**, 2150–2154; (*b*) X. F. Wang, Y. Wang, B. B. Zhang, F. F. Zhang, Z. H. Yang and S. L. Pan, *Angew. Chem., Int. Ed.*, 2017, **56**, 14119–14123; (*c*) X. L. Chen, B. B. Zhang, F. F. Zhang, Y. Wang, M. Zhang, Z. H. Yang, K. R. Poeppelmeier and S. L. Pan, *J. Am. Chem. Soc.*, 2018, **140**, 16311–16319; (*d*) H. P. Wu, H. W. Yu, Z. H. Yang, X. L. Hou, X. Su, S. L. Pan, K. R. Poeppelmeier and J. M. Rondinelli, *J. Am. Chem. Soc.*, 2013, **135**, 4215–4218; (*e*) H. Q. Wu, P. Ju, H. He, B. F. Yang and G. Y. Yang, *Inorg. Chem.*, 2013, **52**, 10566–10570; (*f*) J. H. Huang, C. C. Jin, P. L. Xu, P. F. Gong, Z. S. Lin, J. W. Cheng and G. Y. Yang, *Inorg. Chem.*, 2019, **58**, 1755–1758; (*g*) M. Mutailipu, M. Zhang, B. B. Zhang, L. Y. Wang, Z. H. Yang, X. Zhou and S. L. Pan, *Angew. Chem., Int. Ed.*, 2018, **57**, 6095–6099; (*h*) Z. Z. Zhang, Y. Wang, B. B. Zhang, Z. H. Yang and S. L. Pan, *Angew. Chem., Int. Ed.*, 2018, **57**, 6577–6581.

3 (*a*) D. Phanon and I. Gautier-Luneau, *Angew. Chem., Int. Ed.*, 2007, **46**, 8488–8491; (*b*) F. F. Mao, C. L. Hu, X. Xu, D. Yan, B. P. Yang and J. G. Mao, *Angew. Chem., Int. Ed.*, 2017, **56**, 2151–2155; (*c*) K. M. Ok and P. S. Halasyamani, *Angew. Chem., Int. Ed.*, 2004, **43**, 5489–5491; (*d*) H. M. Liu, Q. Wu, X. X. Jiang, Z. S. Lin, X. G. Meng, X. G. Chen and J. G. Qin, *Angew. Chem., Int. Ed.*, 2017, **56**, 9492–9496; (*e*) Y. J. Jia, Y. G. Chen, Y. Guo, X. F. Guan, C. Li, B. Li, M. M. Liu and X. M. Zhang, *Angew. Chem., Int. Ed.*, 2019, **58**, 17194–17198; (*f*) X. Xu, C. L. Hu, B. X. Li, B. P. Yang and J. G. Mao, *Chem. Mater.*, 2014, **26**, 3219–3230.

4 (*a*) C. F. Sun, C. L. Hu and J. G. Mao, *Chem. Commun.*, 2012, **48**, 4220–4222; (*b*) Z. G. Xia and K. R. Poeppelmeier, *Acc. Chem. Res.*, 2017, **50**, 1222–1230; (*c*) K. M. Ok, *Acc. Chem. Res.*, 2016, **49**, 2774–2785; (*d*) J. J. Zhang, Z. H. Zhang, W. G. Zhang, Q. X. Zheng, Y. X. Sun, C. Q. Zhang and X. T. Tao, *Chem. Mater.*, 2011, **23**, 3752–3761; (*e*) H. S. Ahn, D. W. Lee and K. M. Ok, *Dalton Trans.*, 2014, **43**, 10456–10461; (*f*) C. F. Sun, C. L. Hu, X. Xu, J. B. Ling, T. Hu, F. Kong, X. F. Long and J. G. Mao, *J. Am. Chem. Soc.*, 2009, **131**, 9486–9487; (*g*) T. A. Sullens, P. M. Almond, J. A. Byrd, J. V. Beitz, T. H. Bray and T. E. Albrecht-Schmitt, *J. Solid State Chem.*, 2006, **179**, 1192–1201; (*h*) T. C. Shehee, S. F. Pehler and T. E. Albrecht-Schmitt, *J. Alloys Compd.*, 2005, **388**, 225–229; (*i*) Z. Qian, H. P. Wu, H. W. Yu, Z. G. Hu, J. Y. Wang and Y. C. Wu, *Dalton Trans.*, 2020, **49**, 8443–8447; (*j*) C. Y. Meng, P. Zhang, R. F. Wang and L. Geng, *Dalton Trans.*, 2017, **46**, 12320–12327.

5 (*a*) C. F. Sun, C. L. Hu, F. Kong, B. P. Yang and J. G. Mao, *Dalton Trans.*, 2010, **39**, 1473–1479; (*b*) K. M. Ok and P. S. Halasyamani, *Inorg. Chem.*, 2005, **44**, 2263–2271; (*c*) B. P. Yang, C. L. Hu, X. Xu and J. G. Mao, *Inorg. Chem.*, 2016, **55**, 2481–2487; (*d*) H. Y. Chang, S. H. Kim, K. M. Ok and P. S. Halasyamani, *J. Am. Chem. Soc.*, 2009, **131**, 6865–6873; (*e*) H.-Y. Chang, S.-H. Kim, P. S. Halasyamani and K. M. Ok, *J. Am. Chem. Soc.*, 2009, **131**, 2426–2427; (*f*) Y. H. Kim, T. T. Tran, P. S. Halasyamani and K. M. Ok, *Inorg. Chem. Front.*, 2015, **2**, 361–368.

6 (*a*) Y. Yang, Y. Qiu, P. F. Gong, L. Kang, G. M. Song, X. M. Liu, J. L. Sun and Z. S. Lin, *Chem.–Eur. J.*, 2019, **25**, 5648–5651; (*b*) J. Y. Guo, A. Tudi, S. J. Han, Z. H. Yang and S. L. Pan, *Angew. Chem., Int. Ed.*, 2019, **58**, 17675–17678.

7 (*a*) G. Peng, C. S. Lin, D. Zhao, L. L. Cao, H. X. Fan, K. C. Chen and N. Ye, *Chem. Commun.*, 2019, **55**, 11139–11142; (*b*)

© 2021 The Author(s). Published by the Royal Society of Chemistry

Open Access Article. Published on 10 March 2021. Downloaded on 7/31/2024 3:28:18 PM.
This article is licensed under a Creative Commons Attribution-NonCommercial 3.0 Unported Licence.

X. H. Zhang, B. P. Yang, J. Chen, C. L. Hu, Z. Fang, Z. J. Wang and J. G. Mao, *Chem. Commun.*, 2020, **56**, 635–638.

8 (*a*) C. F. Macrae, I. J. Bruno, J. A. Chisholm, P. R. Edgington, P. McCabe, E. Pidcock, L. Rodriguez-Monge, R. Taylor, J. Van De Streek and P. A. Wood, *J. Appl. Crystallogr.*, 2008, **41**, 466–470; (*b*) P. R. Edgington, P. McCabe, C. F. Macrae, E. Pidcock, G. P. Shields, R. Taylor, M. Towler and J. Van De Streek, *J. Appl. Crystallogr.*, 2006, **39**, 453–457.

9 (*a*) G. M. Sheldrick, *Instruction of Bruker Analytical X-ray Instruments (version 7.60A)*, Bruker Inc., Madison, 2008; (*b*) G. M. Sheldrick, *Acta Crystallogr., Sect. C: Struct. Chem.*, 2015, **71**, 3–8.

10 A. L. Spek, *J. Appl. Crystallogr.*, 2003, **36**, 7–13.

11 (*a*) P. Kubelka and F. Munk, *Z. Tech. Phys.*, 1931, **12**, 593–601; (*b*) J. Tauc, *Mater. Res. Bull.*, 1970, **5**, 721–729.

12 (*a*) B. E. Sørensen, *Eur. J. Mineral.*, 2012, **25**, 5–10; (*b*) X. F. Wang, F. F. Zhang, L. Gao, Z. H. Yang and S. L. Pan, *Adv. Sci.*, 2019, **6**, 1901679.

13 (*a*) B. G. Pfrommer, M. Côté, S. G. Louie and M. L. Cohen, *J. Comput. Phys.*, 1997, **131**, 233–240; (*b*) S. J. Clark, M. D. Segall, C. J. Pickard, P. J. Hasnip, M. J. Probert, K. Refson and M. C. Payne, *Z. Kristallogr. - Cryst. Mater.*, 2005, **220**, 567–570.

14 (*a*) J. P. Perdew, K. Burke and M. Ernzerhof, *Phys. Rev. Lett.*, 1996, **77**, 3865–3868; (*b*) A. Rappe, K. Rabe, E. Kaxiras and J. Joannopoulos, *Phys. Rev. B: Condens. Matter Mater. Phys.*, 1990, **41**, 1227–1230.

15 (*a*) N. E. Brese and M. O'Keeffe, *Acta Crystallogr., Sect. B: Struct. Sci.*, 1991, **47**, 192–197; (*b*) F. F. Zhang, K. Y. Li, H. Ratajczak and D. F. Xue, *J. Mol. Struct.*, 2010, **976**, 69–72.

16 P. S. Halasyamani, *Chem. Mater.*, 2004, **16**, 3586–3592.

17 (*a*) G. Niedner-Schatteburg, *Angew. Chem., Int. Ed.*, 2008, **47**, 1008–1011; (*b*) N. I. Hammer, E. G. Diken, J. R. Roscioli, M. A. Johnson, E. M. Myshakin, K. D. Jordan, A. B. McCoy, X. Huang, J. M. Bowman and S. Carter, *J. Chem. Phys.*, 2005, **122**, 244301.

18 Y. H. Li, G. P. Han, H. W. Yu, H. Li, Z. H. Yang and S. L. Pan, *Chem. Mater.*, 2019, **31**, 2992–3000.

19 (*a*) J. R. Durig, O. D. Bonner and W. H. Breazeale, *J. Phys. Chem.*, 1965, **69**, 3886–3892; (*b*) A. Gajović, I. Friščić, M. Plodinec and D. Ivekovic, *J. Mol. Struct.*, 2009, **924**, 183–191; (*c*) W. G. Nilsen and J. G. Skinner, *J. Chem. Phys.*, 1968, **48**, 2240–2248; (*d*) R. Ma, K. Fukuda, T. Sasaki, M. Osada and Y. Bando, *J. Phys. Chem. B*, 2005, **109**, 6210–6214; (*e*) B. Muthukutty, R. Karthik, S.-M. Chen and M. Abinaya, *New J. Chem.*, 2019, **43**, 12264–12274; (*f*) B. X. Huang, P. Tornatore and Y.-S. Li, *Electrochim. Acta*, 2001, **46**, 671–679; (*g*) A. Manoharan, M. Munusamy, A. Pradeep, S. Sellaiyan, S. Hussain and S. Krishnan, *Appl. Phys. A: Mater. Sci. Process.*, 2020, **126**, 874; (*h*) S. Sharma, H. Pandey, M. Kumar and S. Chhoker, *Superlattices Microstruct.*, 2018, **120**, 161–169.

20 (*a*) Z. B. Cao, Y. C. Yue, J. Y. Yao, Z. S. Lin, R. He and Z. G. Hu, *Inorg. Chem.*, 2011, **50**, 12818–12822; (*b*) R. E. Sykora, K. M. Ok, P. S. Halasyamani and T. E. Albrecht-Schmitt, *J. Am. Chem. Soc.*, 2002, **124**, 1951–1957; (*c*) T. Abudouwufu, M. Zhang, S. C. Cheng, Z. H. Yang and S. L. Pan, *Chem.–Eur. J.*, 2018, **25**, 1221–1226; (*d*) Y. W. An, Y. Zhong, T. Q. Sun, H. J. Wang, Z. P. Hu, H. D. Liu, S. G. Liu, Y. F. Kong and J. J. Xu, *Dalton Trans.*, 2019, **48**, 13074–13080; (*e*) Y. J. Jia, Y. G. Chen, T. Wang, Y. Guo, X. F. Guan and X. M. Zhang, *Dalton Trans.*, 2019, **48**, 10320–10326.

21 A. P. Yelisseyev, L. I. Isaenko and M. K. Starikova, *J. Opt. Soc. Am. B*, 2012, **29**, 1430.

22 Y. H. Li, H. P. Wu, B. B. Zhang, Z. H. Yang, G. P. Han and S. L. Pan, *Inorg. Chem.*, 2018, **57**, 9376–9384.

23 (*a*) O. Mulamba and M. Pantoya, *J. Nanopart. Res.*, 2014, **16**, 2310; (*b*) H. P. Wu, H. W. Yu, W. G. Zhang, J. Cantwell, K. R. Poeppelmeier, S. L. Pan and P. S. Halasyamani, *Cryst. Growth Des.*, 2017, **17**, 4405–4412.

24 (*a*) U. S. Alaan, P. Shafer, A. T. N'Diaye, E. Arenholz and Y. Suzuki, *Appl. Phys. Lett.*, 2016, **108**, 042106; (*b*) H. P. R. Frederikse and G. A. Candela, *Phys. Rev.*, 1966, **147**, 583–584; (*c*) J. M. D. Coey, M. Venkatesan and P. Stamenov, *J. Phys.: Condens. Matter*, 2016, **28**, 485001.

25 (*a*) M. K. Y. Chan and G. Ceder, *Phys. Rev. Lett.*, 2010, **105**, 196403; (*b*) P. J. Hasnip, K. Refson, M. I. J. Probert, J. R. Yates, S. J. Clark and C. J. Pickard, *Philos. Trans. R. Soc., A*, 2014, **372**, 20130270.